Femtosecond laser-induced transformation mechanism from 1D groove structure to 2D microholes structure on the surface of Zr-based metallic glasses

Hanxuan Huang[a,b] , Peilei Zhang[a,b,c1], Zhishui Yu[a,b*], Lei Shen[a,b], Haichuan Shi[a,b], Yingtao Tian[d],

a. School of Materials Engineering, Shanghai University of Engineering Science, Shanghai 201620, China;

b. Shanghai Collaborative Innovation Center of Laser of Manufacturing Technology, Shanghai 201620, China

c. Fraunhofer Institute for Laser Technology ILT, Aachen 52074, Germany

d. Department of Engineering, Lancaster University, Lancaster, LA1 4YW, United Kingdom

Abstract: Laser induced micro-nano texture formation on the surface of solid materials has become a research hotspot in the field of material surface modification. However, due to its extremely easy crystallization characteristics, the study of laser-induced surface modification of bulk amorphous alloy lags behind. In this study, femtosecond laser was used to induce one-dimensional LIPSS (Laser-induced periodic surface structures), SWPSS (Super-wavelength periodic surface structure), a mixed state structure of LIPSS+SWPSS and two-dimensional self-organized microholes structure on surface of the Zr55Cu16Ni15Ti10Al4 bulk amorphous alloy. The numerical difference between LIPSS, SWPSS and self-organized microholes structure in different dimensions such as period, groove width, profile height, etc. were compared, and the roughness of different micro-nano textures and the size of surface undulations were evaluated. The effects of different process parameters on the formation and transformation of micro-nano texture on the surface of zirconium bulk amorphous alloys were investigated. The mechanism of the transformation from LIPSS to SWPSS and finally to two-dimensional self-organized microholes structure was analyzed in detail. Finally, Escherichia coli was cultured on the amorphous surface of Zr-based metallic glasses with different structure. To examine the effect of micro-nano texture on the antibacterial properties of Zr-based metallic glasses surfaces. It is found that the self-organized microholes structure has the best effect in reducing the adhesion of bacteria on the surface of the material.

Keywords: Femtosecond laser, bulk metallic glass, LIPSS, SWPSS, Laser texturing, bacterial adhesion

[1] Corresponding authors: Peilei Zhang (peilei@sues.edu.cn) and Zhishui Yu (yu_zhishui@163.com)

1. Introduction

Amorphous alloy, commonly known as metallic glass, is made by super-rapid solidification. Its atomic distribution has short-range order and long-range disorder, and there are no crystal grains and grain boundaries. Amorphous alloys have excellent corrosion resistance, high fracture toughness, low elastic modulus and superplasticity. They have broad application prospects in the fields of biomedicine, aerospace, etc. For example, Dental implants, orthopedic implants [1] and Spacecraft antenna opening monitoring device [2]. As a member of the large family of amorphous alloys, zirconium-based amorphous alloys not only have the advantages of amorphous alloys, but also have excellent biocompatibility [3] and formability [4]. Besides, their chemical properties are also very stable [5-6]. Therefore, for the field of medical equipment, such as medical scalpels, orthopedic implants and other equipment, zirconium-based amorphous alloys have great research potential [7]. However, the field of medical equipment has very strict requirements on the surface modification of materials. Medical equipment in close contact with the human body, its surface needs to have good antibacterial [8]. Therefore, the surface modification of zirconium-based amorphous alloys has become a research hotspot. Due to the characteristics of amorphous alloys that are very easy to crystallize, the commonly used surface treatment methods for materials cannot perform surface processing on amorphous materials well. Such as: electroplating, sand blasting, shot blasting and other methods have disadvantages such as low processing efficiency, complex technology, and large damage to the substrate[5]. The surface processing of zirconium-based amorphous has become the main reason that limits its wide application. Therefore, it is very necessary to select a suitable surface treatment method for the distinctive amorphous material.

Since the advent of the femtosecond laser, it has attracted worldwide attention due to its extremely short pulse width, ultra-high instantaneous power, micro-nano processing accuracy and almost non-existent thermal effects [6]. It is precisely because of these advantages that femtosecond lasers shine in the field of surface modification of materials. Compared with traditional methods such as electrochemical method and chemical vapor deposition (CVD), femtosecond laser does not involve chemical reagents, has almost no impact on the environment, and is widely applicable to various dielectric materials. Compared with the long pulse width laser, the processing characteristics of femtosecond laser are closer to that of cold processing. The femtosecond laser

will not damage the surface and chemical properties of the material, and can ignore the heat-affected zone, ensuring accurate ablation threshold, high repeatability, high efficiency and high precision ablation geometry control[7-8]. Therefore, femtosecond laser has great research potential in the field of surface modification of amorphous alloys.

Since M.bimbaum et al.[9]first discovered the periodic microstructure of the material surface in 1965, the laser-induced periodic structure of the surface has been extensively studied. However, the advent of femtosecond lasers broke the diffraction limit on the surface of the target material and derives a periodic structure in the micro-nano range. In recent years, femtosecond laser induced periodic micro-nano texture formation on the surface of materials has become a research hotspot. However, due to the characteristics of bulk amorphous alloy that are easy to crystallize and difficult to prepare, compared with other materials, the research progress of femtosecond laser-induced micro-nano texture on amorphous surfaces is relatively lagging. Tomokazu Sano[10] first studied the relationship between $Zr_{55}Al_{10}Ni_5Cu_{30}$ bulk metallic glass femtosecond laser ablation depth and laser pulse energy. The results show that under the pulse energy of the strong ablation zone, the ablation depth of metallic glass is greater than that of crystalline metal. They believe that the thermal electron grain boundary energy loss accelerated by the laser electric field affects the ablation depth of the strong ablation zone. Xinlin Wang et al. [11] studied the femtosecond laser micromachining of zirconium-based bulk amorphous alloys, and determined the ablation threshold of this amorphous alloy through experiments. And they found that the femtosecond laser ablation area does not have defects such as crystallization, melt marks and spatters induced by conventional processing methods near the processing area. This shows that femtosecond laser is a promising amorphization micromachining method. Fengxu Ma et al.[12] studied the evolution of the surface morphology of zirconium-based metallic glass by femtosecond laser ablation. They found that changing the processing parameters can induce different micro-nano textures on the amorphous surface. Lingling Ran[13] used femtosecond lasers to fabricate LIPSS and SWPSSs on amorphous surfaces. Subsequently, more researches on femtosecond laser-induced micro-nano texture on amorphous surfaces were proposed. The research of Cezhi Du et al. [14] proved that treating the amorphous surface into nano-texture can effectively improve the antibacterial and biocompatibility of the surface. Both the Yuhao Lei[15] research group and the Zhen Zhao[16] research group have tried dual-beam femtosecond laser

induced amorphous to obtain highly regular LIPSS. Tie Li[17] found that the use of dual-beam femtosecond lasers with different delays can also make the amorphous surface smoother instead of producing LIPSS. Nowadays, there are more and more researches on femtosecond laser induced texture on bulk amorphous surface. However, it is a pity that although there are many studies on the surface micro-nano texture of femtosecond lasers, few people have prepared one-dimensional LIPSS, SWPSS and two-dimensional microporous structure on amorphous surfaces, and clarified their transformation mechanisms.

In this paper, by continuously experimenting with the process parameters of femtosecond laser, a one-dimensional LIPSS, SWPSS and two-dimensional self-organized microholes structure are induced on the zirconium-based amorphous surface. The effect of laser power, frequency, scanning speed, laser scan number and other process parameters on the micro-nano texture of the amorphous surface was verified, and the mechanism of the one-dimensional to two-dimensional micro-nano texture transformation was proposed and analyzed. The research of femtosecond laser-induced micro-nano texture on the surface of amorphous alloys is of great significance. In addition, the micro-nano structure can effectively inhibit the adhesion of Escherichia coli on the surface of the material, which was found after bacterial culture experiments. This experimental result has played a positive role in promoting the further application of Zr-based metallic glasses in the field of biomedicine.

2. Experiment

2.1 Experimental materials

In this study, a zirconium-based bulk amorphous alloy was selected as the experimental material, and the composition was $Zr_{55}Cu_{16}Ni_{15}Ti_{10}Al_4$. Before femtosecond laser irradiation, the material was processed into a square with a size of 5mm×5mm×2mm by wire cutting. Then we use 320#, 600#, 1000#, 1500# sandpaper to grind and polish the sample surface. A polished sample with a roughness Ra of 0.015 μm was obtained. In the end, the samples were cleaned with ethanol in an ultrasonic cleaning machine for 15 minutes, and then stored in a sealed bag.

2.2 Femtosecond laser experimental method

In this study, an Yb-doped fiber laser system operating at 1030nm (Satsuma HP2, Amplitude, 20W, 40uJ, 300fs) is used as source of femtosecond laser pulses. After placing the sample on the processing platform, the radiation area is selected. The sample surface is irradiated by

femtosecond laser, and the radiation parameter range is as follows:

Table 1 Femtosecond laser radiation parameters

Parameters	Value
Laser power (mW)	6-14
Scan speed (mm/s)	25-100
Pulse frequency (kHz)	10-30
Laser scan number (n)	10-30
Stepover distance between the scan vectors (μm)	10
Focal spot diameter (μm)	25

The stepover distance between the scan vectors is 10 μm, the focal spot diameter is 25 μm, and the area of the processing area is 360 μm×305 μm, the scanning path of the femtosecond laser is shown in Figure 1. Use Keyence's VHX-5000 ultra-depth-of-field microscope (OM) to observe the femtosecond laser radiation area. The S-4300N Scanning Electron Microscope (SEM) of Hitachi Company was used to characterize the two-dimensional micro morphology of the sample surface after femtosecond laser irradiation. The OLS5000-SAF laser confocal microscope (LEXT) of Olympus was used to characterize the 3D nano-level morphology of the sample surface processed by the femtosecond laser, and the change of the height profile of the surface and the size of the surface roughness were measured. Use Panac's XPERT-PRO polycrystalline X-ray diffractometer (XRD) for phase analysis to verify whether the material will crystallize during processing.

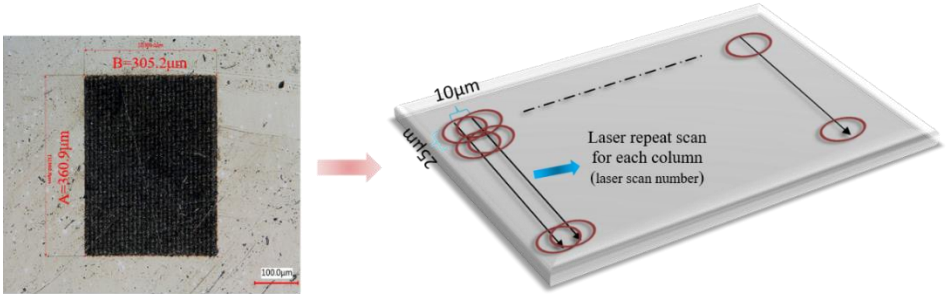

Figure 1 Femtosecond laser scanning path diagram

2.3 Bacterial adhesion experimental method

Prior to bacteria incubate, the sample is placed in an alcohol solvent and then ultrasonically cleaned. After cleaning, the samples were sterilized in a high-temperature sterilization pot at 121 ℃ for 20 minutes. Configure Luria–Bertani (LB) broth and cell suspension. Subsequently, the LB broth was sterilized. Dilute the concentration of the bacterial solution to 10^7CFU/mL with LB broth. The sterilized test samples were added to them separately, and placed in a constant temperature shaker at 37 °C., shaking at 100 rpm for 24 hours. Take out the sample and wash it 3 times with sterile PBS solution at 100 rpm for 5 min. Then add 4% paraformaldehyde to fix for 15 minutes. Finally, use DAPI staining solution to stain at room temperature and avoid light for 15 minutes. After the staining is completed, the staining solution is washed away with saline and photographed with a fluorescence microscope.

3. Results and discussion

3.1 LIPSS, SWPSS and self-organized microholes structure characteristics

The experiment used 3 sets of laser parameters to induce different micro-nano structures on the surface of Ti-based metallic glasses, as shown in table 2. Among them, laser scan number refers to the number of repetitions of each column of laser scanning in the raster matrix (Figure 1). Using raster mode to repeatedly scan the substrate (Figure 1) will induce different micro-nano structures on the surface. In the raster mode, the spot diameter is 25 μm and the line spacing is 10 μm. Under the femtosecond laser radiation of parameter group 1, 2, 3: LIPSS, SWPSS and two-dimensional self-organized pore structures were found on the surface of the material.

Table 2 Experimental parameter table

Parameters	1	2	3
Laser power (mW)	6	12	14
Scan speed (mm/s)	100	100	25
Pulse frequency (kHz)	10	30	10
Laser scan number (n)	10	10	10
Effective accumulated fluence of a single pulse (J/cm^2)	0.23	1.38	2.16

Accumulated fluence in the radiation area (J/cm^2)	31.92	191.52	299.78
Micro-nano structure	LIPSS	SWPSS	Proe structure

Figure 3 is a scanning electron microscope image of the zirconium-based amorphous surface after scanning with a femtosecond laser. As shown in Fig. 2, the red arrow in the upper right corner is the direction of the femtosecond laser polarization. As shown in Fig. 2a, no structure can be found on the polished surface. As shown in Fig. 2b, LIPSS is arranged perpendicular to the laser polarization direction with a period of approximately 830 nanometers. The width of each ripples of LIPSS is 240 nanometers, and the length is the scan length. As shown in Fig. 2c, compared with LIPSS, the direction of the SWPSS grooves is deflected by 90°, forming a micro-nano structure periodically arranged horizontally. Compared with LIPSS, the period of SWPSS is larger, reaching 2930 nm, and the groove width is 720 nm. Although continuous in the length direction, there is a layer of faint dislocation of the line every 10 μm (about the scanning pitch). To sum up, since the size and period of the LIPSS and SWPSSs are formed only in the width direction, they are called one-dimensional structures. As shown in Fig. 3d, the structure of self-organized holes is a series of neatly arranged micro-pores. Each column of self-organized holes has periodicity, and its period is 10.12 μm. The diameter of the holes is 2.3 μm, and the distance between two adjacent holes in each column is 4.3 μm. The size and period of self-organized micropores are formed in both the length and width directions, so it is called a two-dimensional structure.

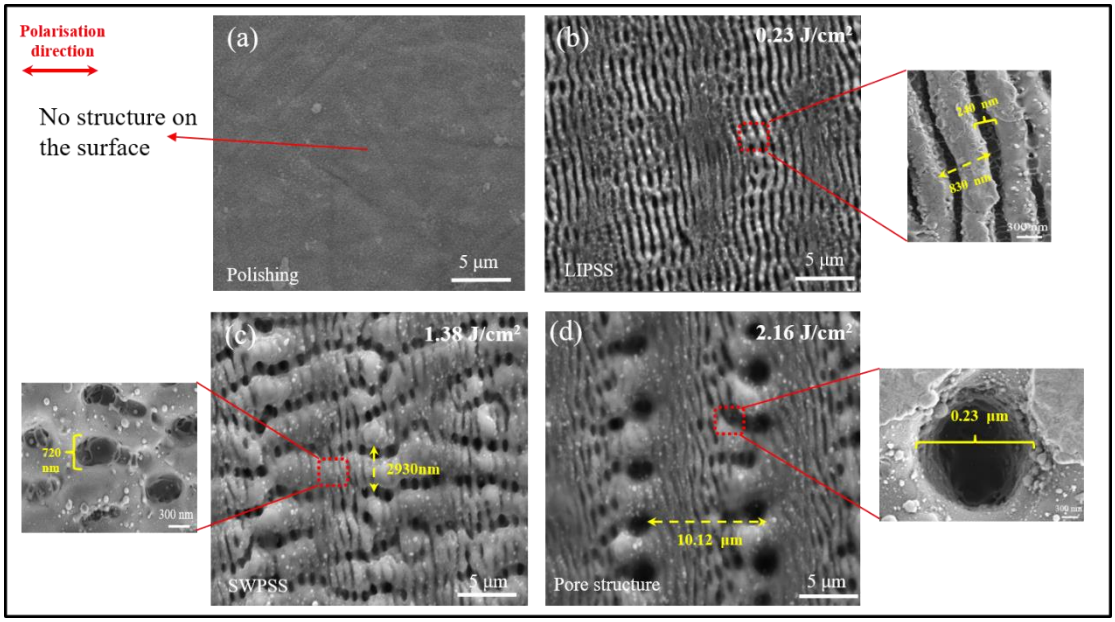

Figure 2 Scanning electron micrograph of Polishing, LIPSS, SWPSS and self-organized microholes structures

3.2 The influence of different parameters on micro-nano texture

In order to study the characteristics of micro-nano texture induced by femtosecond laser radiation of zirconium-based metallic glass. The parameters in experiment group 1 were used for research (Figure 3), the micro morphology under different laser power and scanning speed was first observed. As shown in Figure 3, the red arrow in the upper right corner is the direction of the femtosecond laser polarization. In experimental parameter group 1, the parameter array distribution of the experimental group, each row from left to right, the effective accumulated fluence (single pulse) decreases; each column from top to bottom, the effective accumulated fluence increases. The calculation method of the effective accumulated fluence (single pulse) is shown in formula (6). Therefore, it can be seen that the green box in the parameter array is the parameter with the lowest effective accumulated fluence, and the red box is the parameter with the highest effective accumulated fluence. It can be seen from the morphological characteristics of experimental group. When the effective accumulated fluence is 0.23 J/cm^2, LIPSS is found on the surface of the material. Increasing the effective accumulated fluence to 0.38 J/cm^2, the micro-nano texture of the zirconium-based amorphous surface initially evolved from a one-dimensional LIPSS to a LIPSS + SWPSS. At this time, the SWPSS has just been formed and it is not obvious yet. When the effective accumulated fluence to 0.92 J/cm^2, the micro-nano texture then evolved into a

SWPSS + LIPSS. At this time, the SWPSS is already very obvious, and a small amount of LIPSS remains on the surface. With the effective accumulated fluence increase to 1.08 J/cm^2, the micro-nano texture has completely evolved from the SWPSS + LIPSS to a SWPSS. Continuously increasing the effective accumulated fluence, the surface of the zirconium-based metallic glass will gradually form a hole-like structure. When the effective accumulated fluence is 2.16 J/cm^2, the two-dimensional self-organized microholes structure is found on the surface of the material. Observing the surface morphology ~~of each column~~ in experimental group 1, increasing the effective accumulated fluence will induce the micro-nano texture to evolve from one-dimensional LIPSS to two-dimensional self-organized microholes structure.

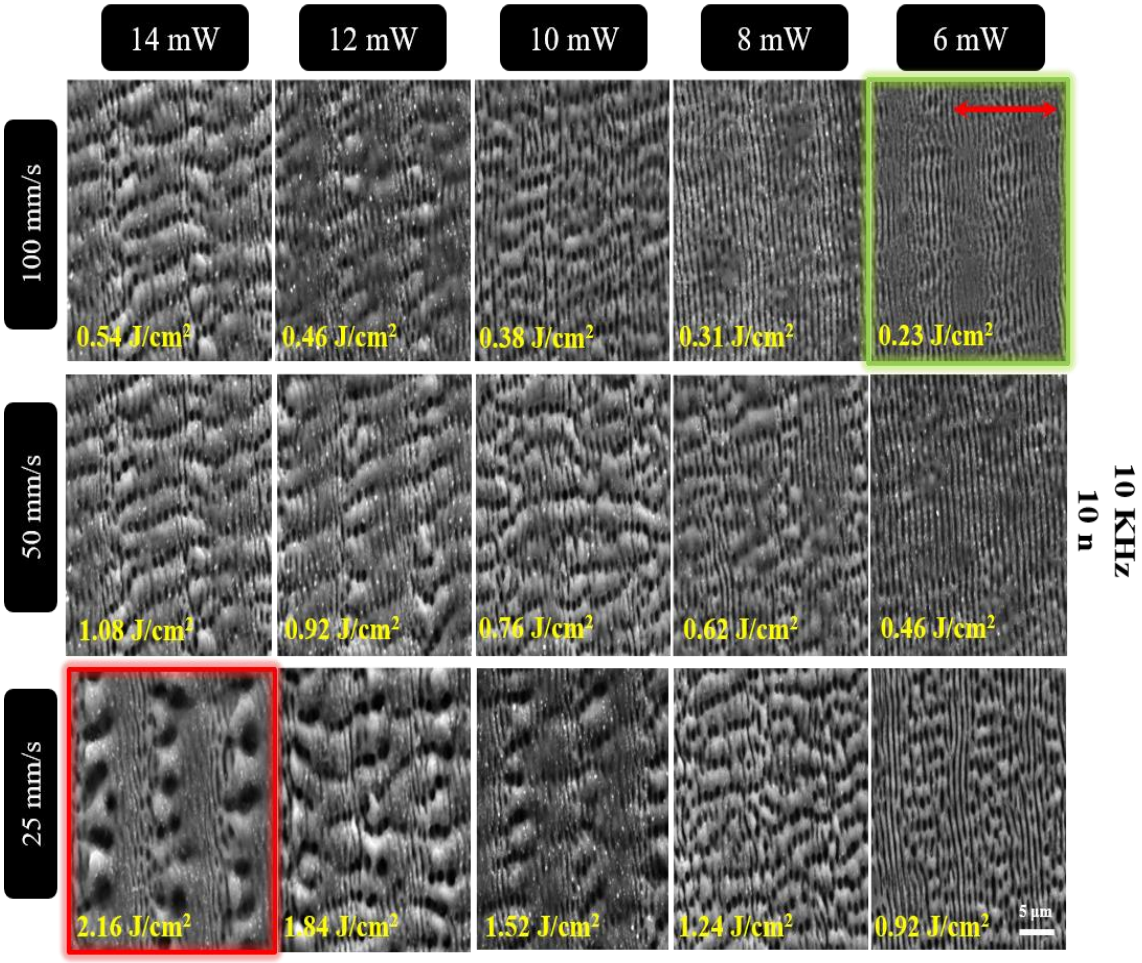

Figure 3 Experimental group 1: The evolution of surface topography under different laser power and scanning speed under femtosecond laser irradiation

From the experimental process, increasing the laser power or reducing the scanning speed can increase the effective accumulated fluence (as shown in the third row or fourth column of Figure 3). The increase of effective accumulated fluence will not only cause the transformation of

the micro-nano structure, but also increase the amplitude of the micro-nano structure. In order to verify this point of view, we used an atomic force microscope to observe the amplitude of the Zr-based metallic glasses surface under different effective accumulated fluence. As shown in Figure 4, when the effective accumulated fluence is 0.23 J/cm^2. We observe that the amplitude (the distance from the peak to the trough in the height curve) of the micro-nano structure is small, the amplitude is 120nm. When the effective accumulated fluence reaches 0.62 J/cm^2, the surface structure has changed from LIPSS to SWPSS. The change period of the amplitude in the figure is obviously longer, and the fluctuation is more obvious. When the effective accumulated fluence is 1.08 J/cm^2. We observe that SWPSS has formed on the surface of the material. The amplitude of the micro-nano structure becomes larger, reaching 450nm.When the effective accumulated fluence reaches 2.16 J/cm^2, Two-dimensional microporous structure is found on the surface of the material. The amplitude of the micro-nano structure reaches its peak, and the fluctuation is more obvious. The amplitude of the two-dimensional microporous structure reaches 700nm.

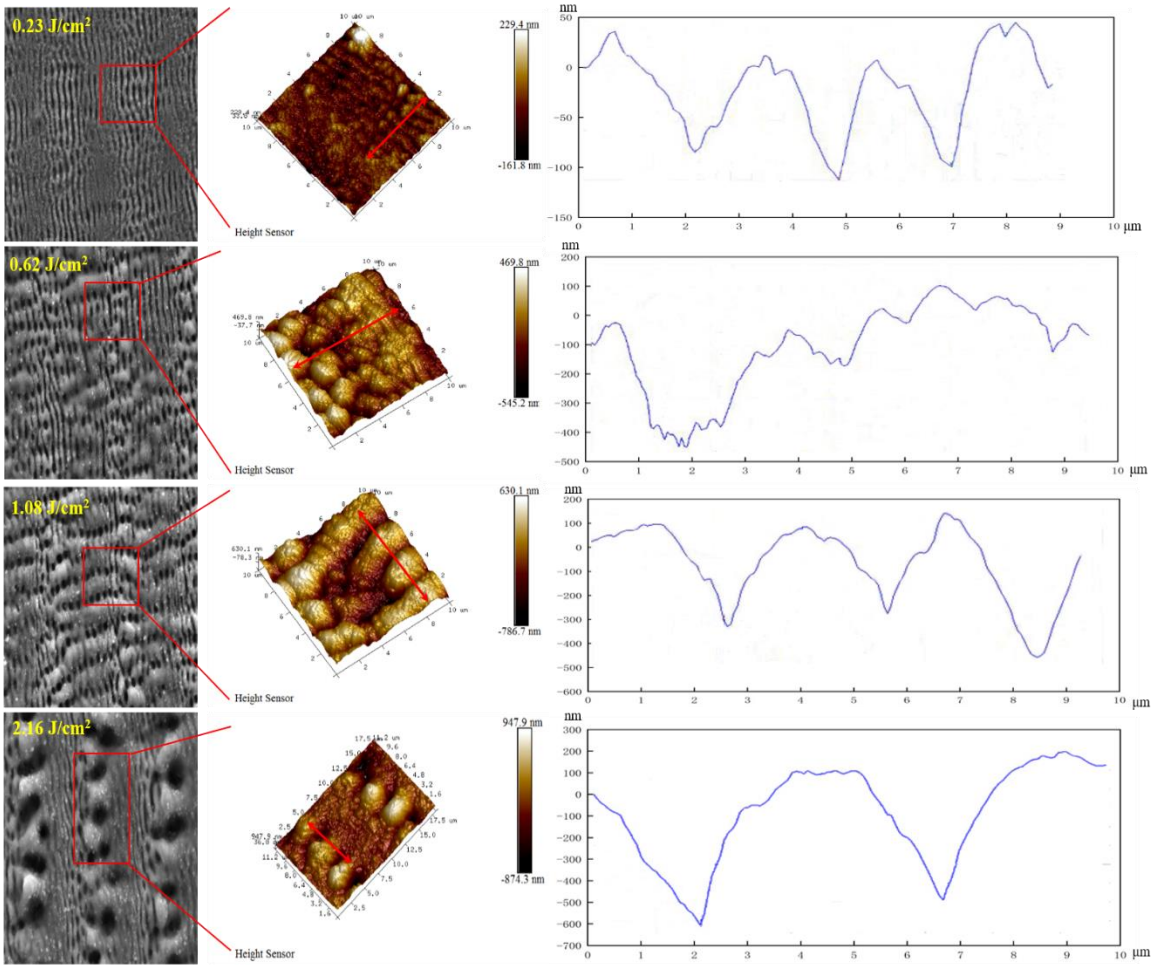

Figure 4 Zr-based metallic glasses surface hight profile with different effective accumulated

fluence

In order to further study the influence of main parameters such as pulse frequency and laser scan number on the micro-nano texture of the zirconium-based amorphous surface. The parameter arrays of experimental group two and three were set up (Figure 5, 6). As shown in Figure 5, the parameter array of experimental group 2 is similar to experimental group 1, the laser power parameter interval of each row is the same, and the pulse frequency of each column increases from top to bottom. The parameter array distribution of the experimental group, each row from left to right, the effective accumulated fluence (single pulse) decreases; each column from top to bottom, the effective accumulated fluence increases. It can be seen that at a lower effective accumulated fluence, increasing the effective accumulated fluence will induce the micro-nano texture of the material surface from a one-dimensional LIPSS to a LIPSS + SWPSS. At this time, SWPSS has just formed. At higher effective accumulated fluence, increasing the effective accumulated fluence will induce the micro-nano texture to transform from LIPSS + SWPSS to SWPSS. When the effective accumulated fluence reaches a certain threshold, self-organized microholes are formed. Interestingly, a small increase in the effective accumulated fluence will also increasce the amplitude of the micro-nano texture. As shown in Figure 6, the parameter array of experimental group 3 controls the change of the laser scan number and the laser power. The laser power change interval of each row is the same as that of experimental groups 2 and 3. The laser scan number in each column increases continuously from top to bottom. Increasing the laser scan number is similar to increasing the pulse frequency. A small increase will cause the micro-nano texture amplitude to increase, and a large increase will induce the micro-nano texture to shift from LIPSS to SWPSS, and finally form a self-organized microholes structure.

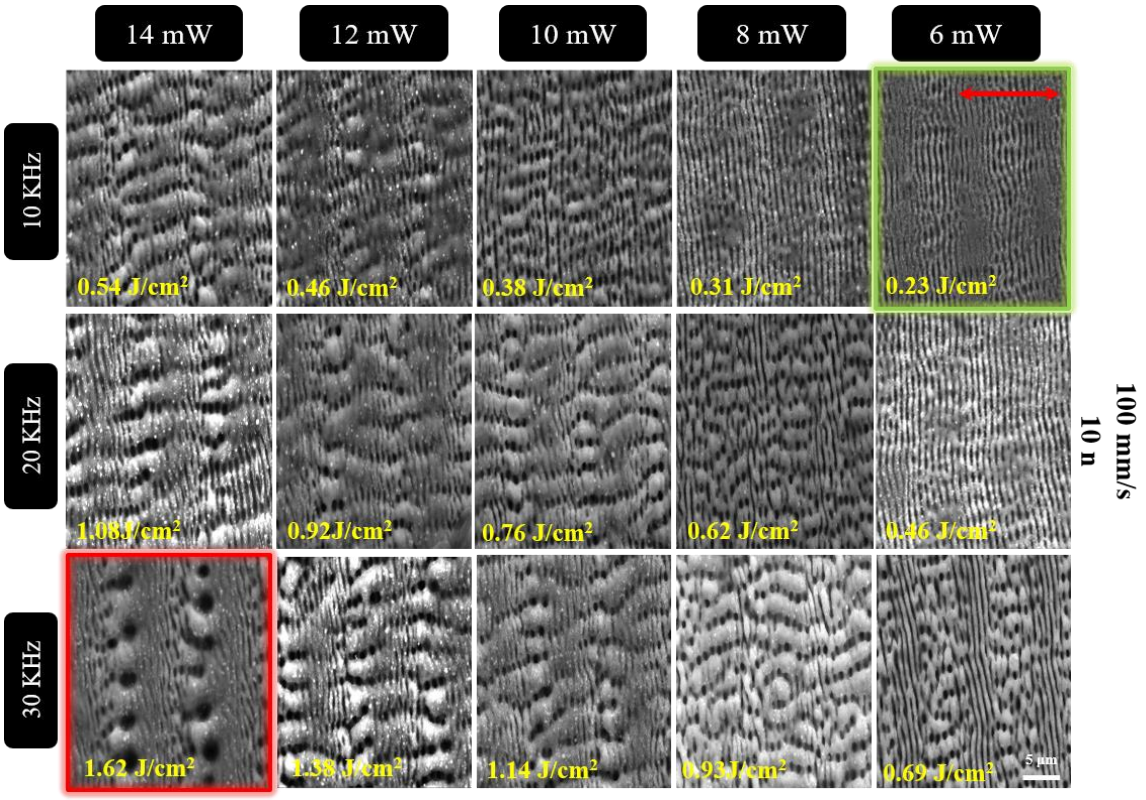

Figure 5 Experimental Group 2: Evolution of surface topography under different laser power and pulse frequency under femtosecond laser irradiation

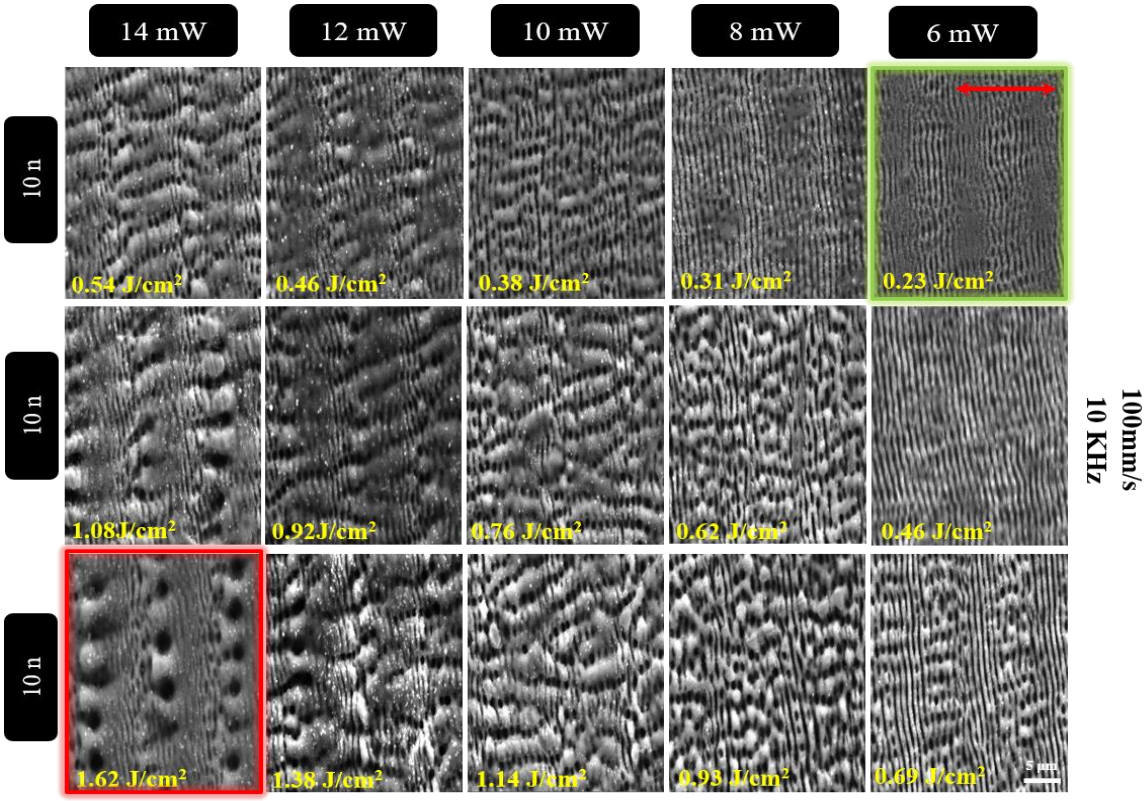

Figure 6 Experimental group 3: Evolution of surface topography under different laser power and laser scan number under femtosecond laser irradiation

In general, increasing the effective accumulated fluence will induce the micro-nano texture of the material surface to gradually change from one-dimensional LIPSS to SWPSS. Finally, it completely evolved into a two-dimensional self-organized microholes structure. A small increase in these parameters will deepen the amplitude of the micro-nano texture.

3.3 LIPSS to SWPSS transition mechanism

In previous studies, the main physical mechanisms of the femtosecond laser-induced LIPSS formation on the material surface are the Sipe-Drude theory[18-21] and the SSP theory[22-24]. The theory that induces the SWPSS is mainly the thermal capillary convection effect[25-27]. However, there is no detailed study on the mechanism of femtosecond laser-induced LIPSS conversion to SWPSS and self-organized microholes structure on amorphous surfaces. This article will elaborate and explain its transformation mechanism in depth.

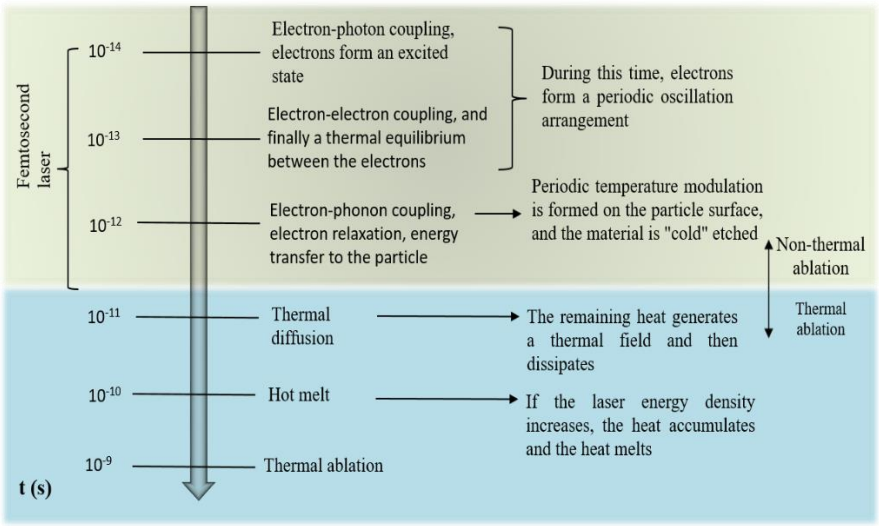

Figure 7 Time axis of interaction between femtosecond laser and solid material[28]

As we all know, the pulse width of a single femtosecond laser is extremely short, reaching the order of 10^{-15}s, and this is one of the characteristics that makes the femtosecond laser stand out. The ultra-short pulse width and extremely high instantaneous power density make the time (t_L) for free electrons on the surface of the material to change from an equilibrium state to an excited state (t_L) when the femtosecond laser is processing solid materials is much shorter than the electron-phonon scattering and the lattice heating Time ($t_{ep}=10^{-12}$s). It is this point that distinguishes the "cold working" characteristic of femtosecond lasers. At the same time, this also shows that at lower energy density, the entire reaction process of femtosecond laser-induced micro-nano texture on the surface of solid materials is completed before t_{ep}. We will use the

timeline of Figure 7 to describe the mechanism of LIPSS turning into SWPSS.

It can be seen from the dual temperature model that metal materials can be simplified into a lattice system and a surface free electron system[29]. For amorphous alloys, we modify the model. As shown in Figure 8b, we believe that amorphous alloys consist of a free electron system on the surface and a short-range ordered and long-range disordered atomic system. When the hand of the time axis is slowly pushed, the femtosecond laser radiates the amorphous alloy. At this time, the femtosecond laser takes the lead to act on the free electron system on the surface of the material, and interfere with the electromagnetic wave generated by the free electron system on the surface of the material. At the same time, the photon and the electron are coupled, and the electron absorbs energy to become an excited state. This process corresponds to the time $t=10^{-14}$ in the time axis of Figure 7. Then the electron-electron coupling, as shown in Figure 8c, finally makes the temperature and density of the electrons periodically oscillate ($t=10^{-13}$). Then, before $t=10^{-12}$ order of magnitude, the electrons couple with the phonons in the amorphous alloy, and the electrons relax. The electron transfers energy to the atomic system of the amorphous alloy (Figure 8b), forming a periodic modulation of the energy on the surface of the material. The material in the high-energy deposition zone is etched and ripples are generated on the surface. In the low energy zone, the deposited energy is not enough to remove the surface of the material. Therefore, one-dimensional LIPSS appeared. In the process of forming LIPSS, since the pulse width of the femtosecond laser is much smaller than the t_{ep}, the energy deposited in the electrons cannot be completely transferred to the atomic system, and the laser radiation ends. At this time, the temperature of the electrons is very high, but the temperature of the atoms is still very low. The electrons remove the material through avalanche ionization and breakdown. Therefore, the process of forming one-dimensional LIPSS on the surface of the amorphous alloy induced by the femtosecond laser has almost no thermal effect and is almost cold etching.

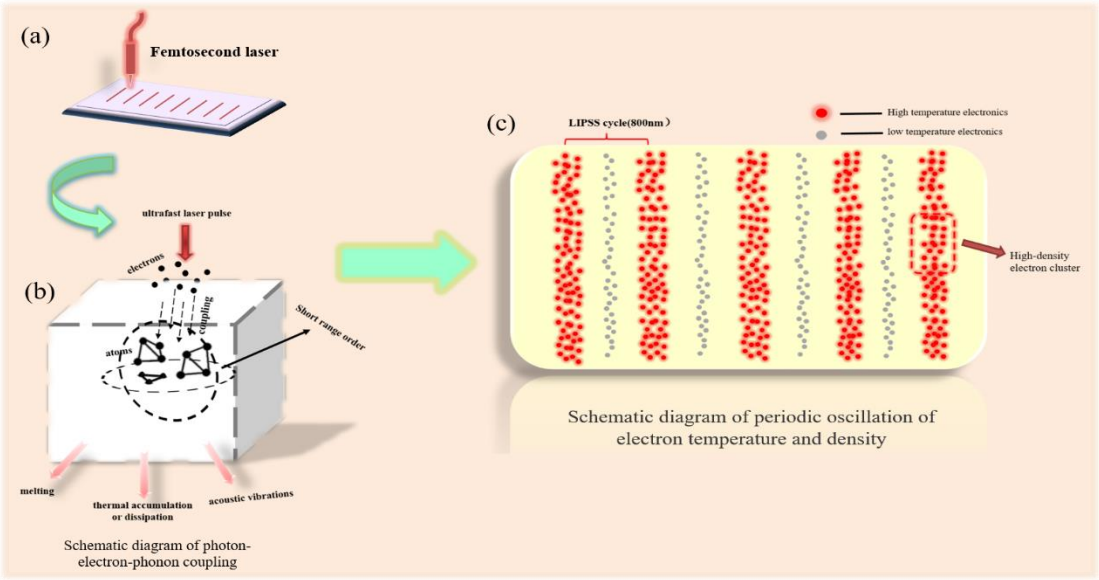

Figure 8 Schematic diagram of photon-electron-phonon coupling in amorphous alloys and periodic oscillation of electron temperature and density on the surface of the material

It is known from the time axis that the time of photon-electron, electron-electron, and electron-phonon coupling is much shorter than the time of thermal diffusion. Therefore, after the end of the interaction between the femtosecond laser and the amorphous crystal, the remaining energy is mainly diffused in the form of thermal and acoustic energy (Figure 8b). The remaining thermal energy will remain on the surface of the amorphous alloy and diffuse into a thermal field. We can define the energy of this thermal field as x. Obviously, the thermal field energy x at this time is much smaller than the melting threshold of the material and is not enough to cause thermal melting. In this case, it can be explained why the changes of laser power, pulse frequency, scanning speed and laser scan number cause the micro-nano texture of the amorphous alloy surface to gradually transition from LIPSS to SWPSS. Taking the pulse frequency as an example, a femtosecond laser with a low pulse frequency is used for processing, and the time interval between each pulse is longer. Therefore, before the next pulse acts on the surface of the material, the energy of the residual thermal field in the laser focus area has enough time to gradually diffuse and disappear. Once the pulse frequency is increased, the energy of the thermal field will not be able to diffuse out in the future, and the next pulse will be input, so that the energy x of the thermal field will gradually accumulate. This phenomenon is the cause of the increase in accumulated fluence. With the increasing of accumulated fluence, the energy of the thermal field brought by multiple pulses forms a thermal accumulation effect until the thermal accumulation

and thermal diffusion reach equilibrium, assuming that the energy of the thermal field is y at this time. And y is proportional to the accumulated fluence. Increasing the accumulated fluence will increase the thermal field energy y, and vice versa. Pulse frequency, laser power, scanning speed, laser scanning number and other laser parameters will cause changes in accumulated fluence. The increase in accumulated fluence is the cause of the heat accumulation effect. At this time, if the value of y reaches the melting threshold of the material, the material starts to remelt, as shown in the slightly remelted area in Figure 11(a). In order to explain this phenomenon, we simulated the temperature field of Zr-based metallic glasses during a femtosecond pulse period. In this temperature field model, all parts of the material transfer heat uniformly. The model size is 0.4mm×0.25mm×0.1mm. The model is divided into free tetrahedron meshes, the smallest mesh element size is 1/4 of the spot diameter, and the ambient temperature is 25℃. Using a fixed Gaussian distribution laser as a heat source to load on the surface of the material, the energy density distribution function of a single pulse is as follows[30]:

$$\boldsymbol{\Phi}(x,y,t)=\frac{\alpha p}{\pi\omega^2}\exp[-2\frac{(x-x_0)^2-(y-y_0)^2}{\omega^2}]\exp[-2\frac{(t-t_w)^2}{t_w^2}] \quad (1)$$

In the formula: p is the laser power, ω is the spot radius, t is the heat source loading time, t_w is the laser pulse width, and α is the absorption rate of the laser light on the surface of the material.

The process of heat conduction in this experiment follows the heat conduction equation based on Fourier law and energy conservation[31] :

$$\kappa\left(\frac{\partial^2 T_S}{\partial x^2}+\frac{\partial^2 T_S}{\partial y^2}+\frac{\partial^2 T_S}{\partial z^2}\right)=\rho c\frac{\partial T}{\partial t} \quad (2)$$

In the formula, κ is the thermal conductivity of the material, Ts is the instantaneous temperature of the material, t is the heat transfer time, and ρ and c are the density and specific heat capacity of the material.

The temperature field of Zr-based metallic glasses in a pulse period is simulated when the laser power is 6 mW (90fs-350fs after femtosecond laser radiation). In addition, the three-dimensional isotherm model of Zr-based metallic glass at 90 fs after femtosecond laser irradiation is extracted (figure 10). As shown in Figure 9, laser pulses act on the surface of Zr-based metallic glasses. The temperature rises instantaneously, and the material is first removed from the center of the spot. After the laser pulse is over, there is no continuous heat source, and the heat diffuses to the surroundings (Figure 9). Therefore, the surface temperature will drop

rapidly. If the next pulse is applied to the surface of the Zr-based metallic glasses before the heat is completely diffused, heat accumulation will be formed. This confirms the previous hypothesis that when the heat buildup is large enough, it will induce micro-remelting on the surface of the material. Finally, a SWPSS, even a two-dimensional self-organized microholes structure is formed.

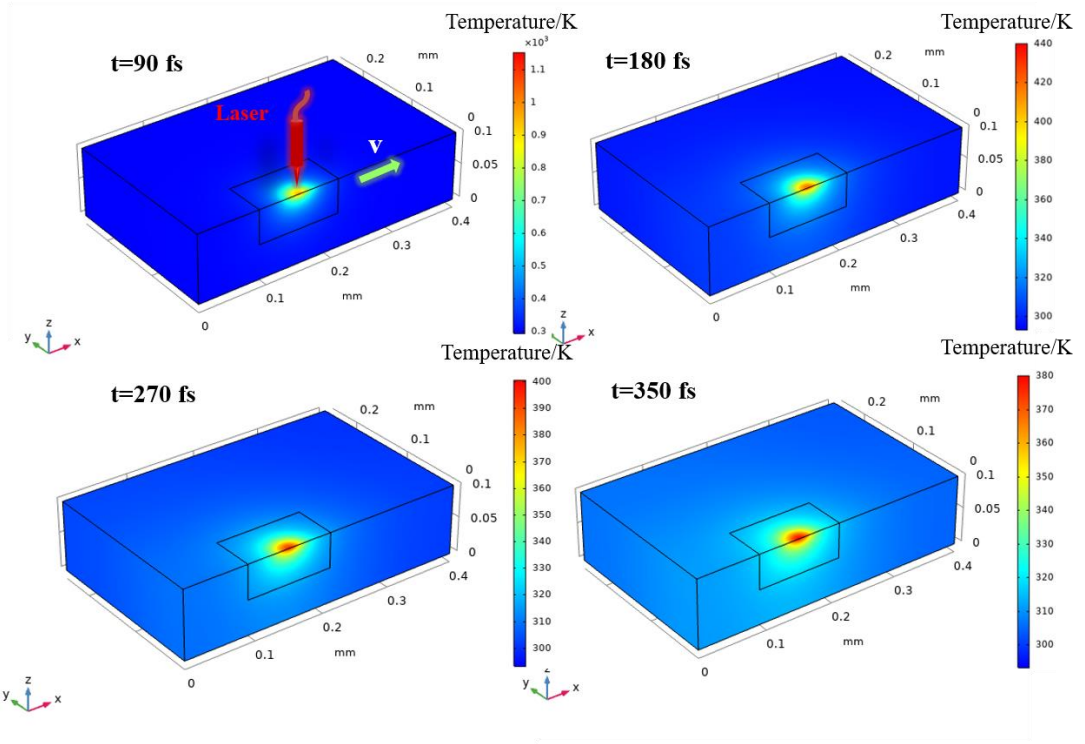

Figure 9 Simulation diagram of temperature field in a pulse cycle

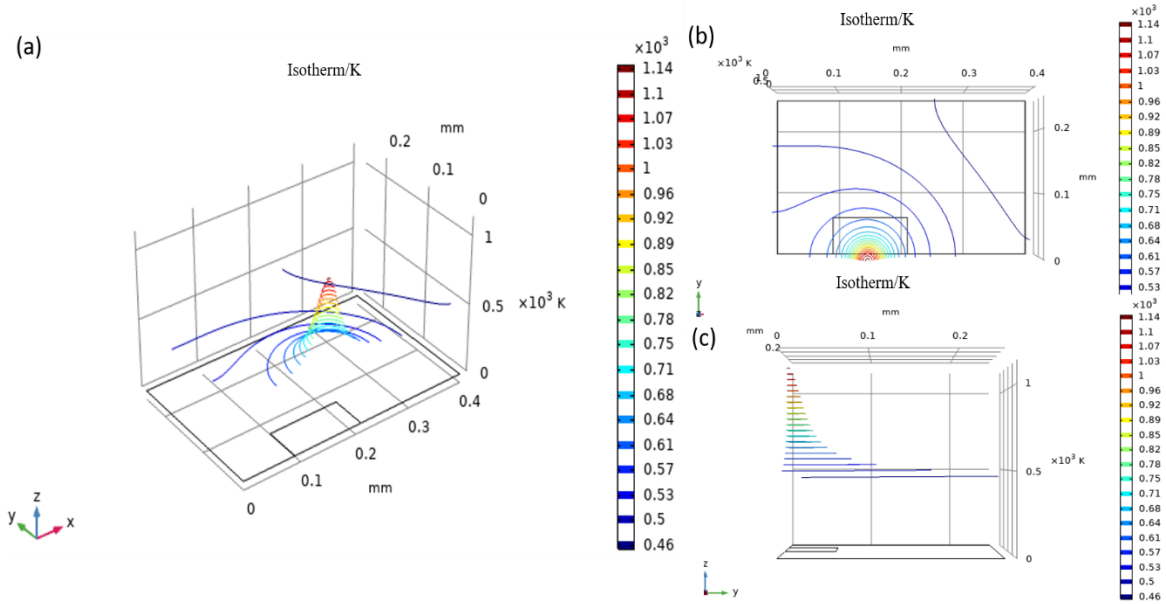

Figure 10 3D isotherm simulation diagram of Zr-based metallic glasses: (a)

three-dimensional view of isotherm (b) top view of isotherm (c) side view of isotherm

When the accumulated fluence reaches the material's remelting threshold, the micro-nano structure changes from LIPSS to SWPSS. At the beginning of the remelting process, the temperature of the amorphous alloy surface showed a gradient distribution similar to LIPSS. However, heat is more likely to accumulate at the ripple, so that the solid amorphous on the two sides of the ripple wall starts to melt first. At this time, since the temperature gradient is not much different, and the matrix has just begun to remelt, the effect of Marangoni thermal convection is not obvious. Therefore, the gravity of the micro-melt droplets plays a dominant role. The micro-melt droplets formed on the two sides of the ripple wall slide into the bottom of ripple and then stick together to block the ripple to form a section of the groove (horizontal to the polarization direction). Subsequently, due to gravity continues to play a leading role, the micro-melt droplets continuously slide into the ripple, and the ripple is continuously filled, gradually filling from a long strip to an oblate. For the horizontal arrangement, since from the beginning, the two horizontal sides of the trench are platforms. The droplets here did not slide into the ripple in time. With the rapid increase in temperature, the surface tension of the micro-melt pool is greater than its gravity, and with the action of electromagnetic force, the micro-melt has no chance to slide into the ripple. The pits are ablated laterally (the pits have a tendency to induce the formation of pits laterally). The research of George D. Tsibidis[25]et al. confirmed this point. They found that the micro molten pool has a large velocity component in the horizontal direction through simulation. Finally, under the combined action of electromagnetic interference, Marangoni thermal convection effect and gravity, the horizontal groove SWPSS was formed. However, since the edges of the groove are constantly being melted, heat is more likely to accumulate at the groove. At this time, the Marangoni thermal convection effect began to gradually play a leading role, because the temperature at the ripple is higher than the surroundings, and a temperature gradient with the groove as the boundary is formed with the surroundings. For liquids, the higher the temperature, the lower the surface tension. Under the effect of Marangoni heat convection, the liquid with low surface tension will flow to the liquid with high surface tension. As the temperature gradient between the trench and its surroundings continues to increase, the surface tension gradient will also continue to increase until the surface tension of the micro-melt pool and the gravity of the micro-melt droplets and the surface electromagnetic force

of the material reach a balance. Finally, a neatly arranged microporous structure is formed. The energy density continues to increase. The horizontal groove continues to be melted. Under the effect of Marangoni convection, the grooves form a row of neatly arranged circular hole-like structures.

In order to verify this hypothesis, we set up a set of experimental parameters that change the accumulated fluence. As shown in Figure 11, as the accumulated fluence to increase, the heat accumulation energy y continues to increase. The surface structure of amorphous alloys gradually changes: (a) LIPSS started to micro remelting (b) Part of LIPSS is remelted to form LIPSS+ SWPSS (c) The remaining LIPSS are further remelted to form micro-pits, forming a transition state structure of LIPSS+SWPSS (d) SWPSS + a small amount of remaining LIPSS, thermal ablation is completed (e) The energy input is too high, and the micropits of SWPSS begin to expand and swallow each other, Finally formed an array of holes. Due to the incomplete expansion of the experiment, it is expected that the energy input will continue to increase, and the lateral micropits in the SWPSS will swallow each other, eventually forming a microholes structure.

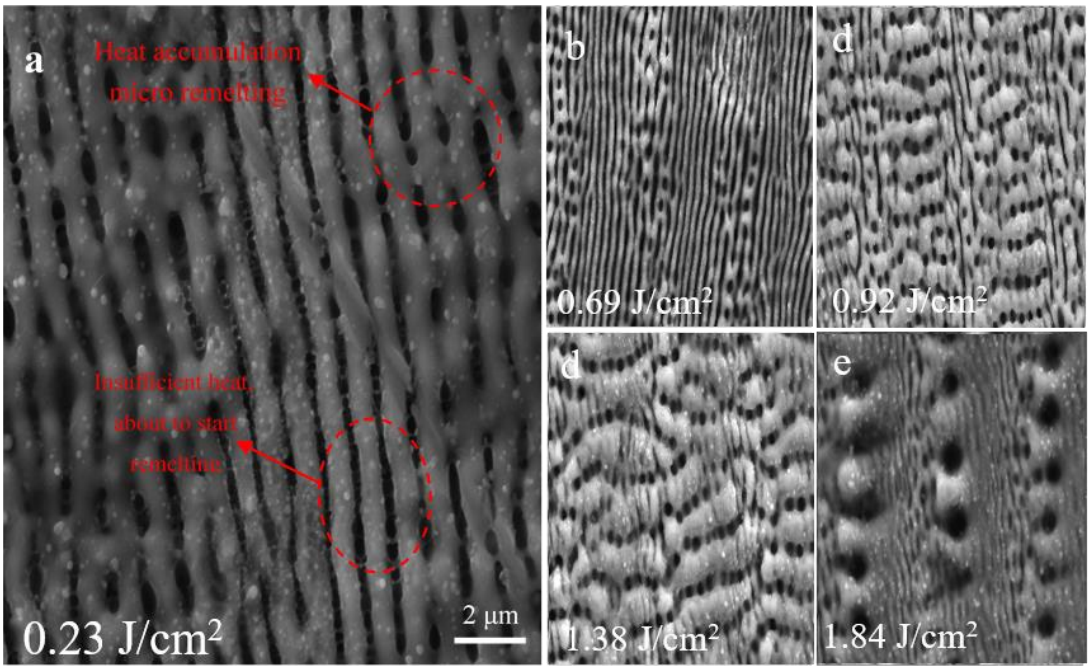

Figure 11 Micro-nano texture changes under different accumulated fluence

In the same way, increasing the laser power, the laser scan number, and reducing the scanning speed will also cause a thermal accumulation effect, leading to a continuous increase in y, and

ultimately changing the surface texture. In order to express this effect more clearly, we can use the following formula[32] to quantitatively explain:

Energy density of single spot:

$$\Phi=\frac{E}{\pi\omega^2} \quad , \quad E=pt_w \tag{3}$$

Line scan, when the laser scan number = 1, the effective pulse number at a single spot:

$$PPS=\frac{2\omega f}{u} \tag{4}$$

When scanning, the laser scan number=1, the effective pulse number at a single spot:

$$PPS_{tot}=PPS\frac{2\omega}{H}=\frac{4\omega^2 f}{uH} \tag{5}$$

Effective accumulated fluence of a single pulse:

$$\Phi_{tot}=PPS_{tot}\Phi=\frac{4nfpt_w}{\pi uH} \tag{6}$$

The total number of pulses in the radiation area:

$$P_n=n_1n_2=\frac{nAf(B-H)}{u(2\omega-H)} \tag{7}$$

Total accumulated fluence in the radiation area:

$$\Phi_{acc}=P_n\Phi=\frac{nAfpt_w(B-H)}{\pi u\omega^2(2\omega-H)} \tag{8}$$

Where p is the femtosecond laser power, t_w is the laser pulse width, E is the laser input energy, Φ is the energy density of a single spot, and ω is the spot radius of a single spot. PPS is the number of effective pulses at a single spot when the laser is scanned in a single line, f is the femtosecond laser frequency, and u is the scanning speed of the laser. PPS_{tot} is the number of effective pulses at a single spot when the entire surface is scanned, and H is the stepover distance between the scan vectors (Figure 1). Φ_{tot} is the effective accumulated fluence of a single pulse in the experiment, and n is the laser scan number. By the formula (6) can be seen, increasing the laser power, pulse frequency and number of elements, or decrease the scanning speed, the effective accumulated fluence at a single spot can be increased. In formulas (7) and (8), P_n is the total number of pulses in the laser radiation area. n_1 is the number of pulses in each column of the radiation matrix, n_2 is the number of columns in the radiation matrix. A is the length of the radiation matrix, B is the width of the radiation matrix (as shown in Figure 1). By formula (8), the total accumulated fluence in the radiation area can be calculated. When the effective accumulated fluence reaches a certain threshold, it will eventually cause the thermal accumulation effect of the

amorphous surface, causing the LIPSS on the material surface to micro-remelt, and finally transform into the SWPSS and two-dimensional self-organized microholes structure.

According to the formula, the variation curve of the effective accumulated fluence in a single spot with various parameters can be listed. Take the laser power parameter as an example, as shown in Figure 12. From Figure 12 we can more intuitively find the influence of laser power on the effective accumulated fluence and the final influence on the micro-nano texture of the amorphous surface. In the same way, the effect of scanning speed, laser frequency and laser scan number on the effective accumulated fluence can be obtained. Therefore, this article will not repeat the description too much.

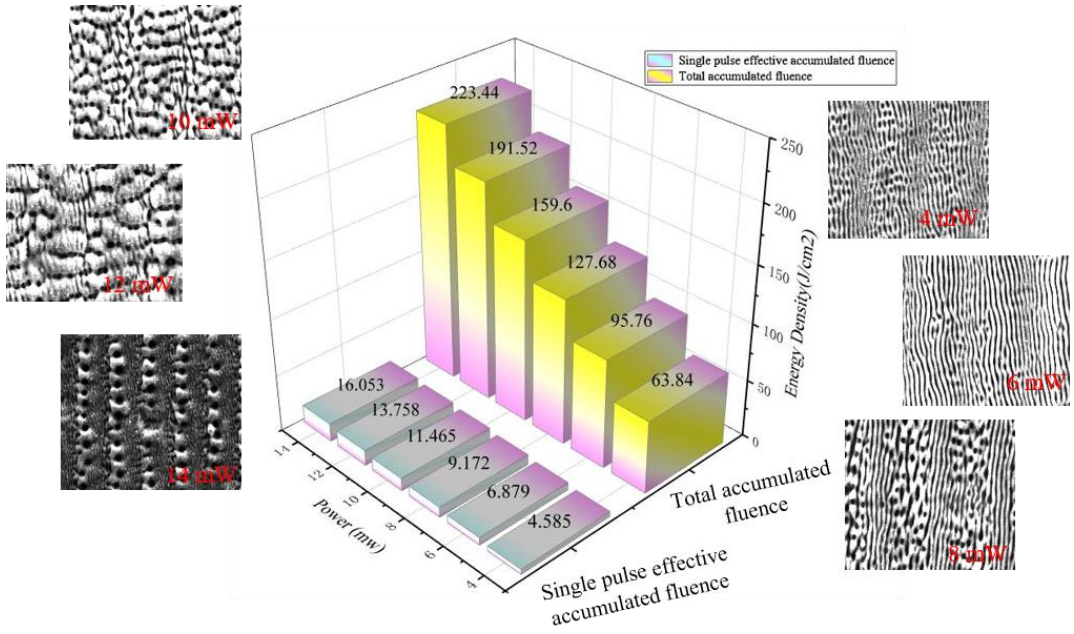

Figure 12 The influence of laser power on single pulse effective accumulated fluence and total accumulated fluence

3.4 Surface properties of different micro-nano structures

3.4.1 Surface morphology and surface roughness

In order to better study the effect of different surface structures on the properties of Zr-based metallic glasses surfaces. We have carried out experimental tests on the three-dimensional morphology, roughness and antibacterial properties of the sample surface. Figure 13(a,b,c) shows the 3D micro-morphology and height profile change curves of three micro-nano textures on the amorphous surface. It can be seen that whether it is one-dimensional LIPSS, SWPSS or two-dimensional microporous structure, its height profile distribution also has periodic changes.

And this periodic change is in step with the periodic change of its surface structure. In addition, the height profile fluctuations of LIPSS, SWPSS and the hole structure increase in turn. The period of the height profile fluctuations also gradually becomes larger.

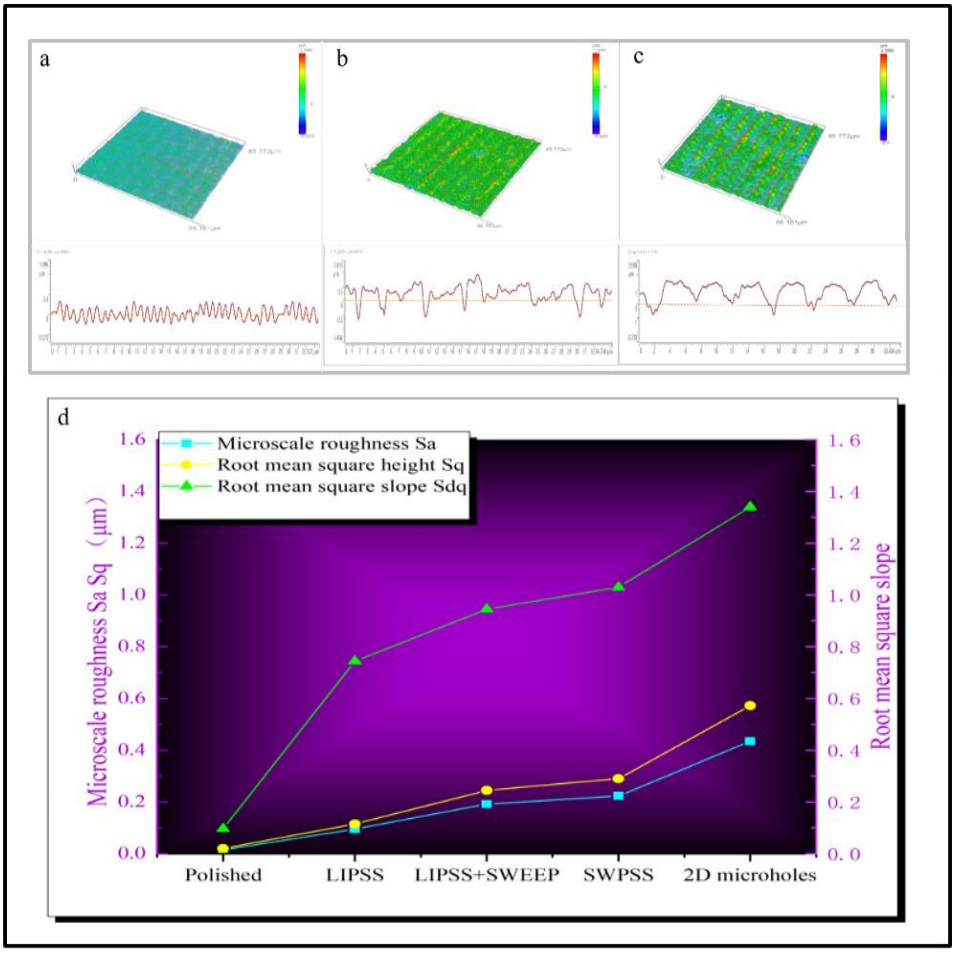

Figure 13 Confocal laser scanning microscope scans the three-dimensional micro-topography and roughness measurement values of different surface structures

In order to compare the surface undulation degree of different micro-nano textures, the laser confocal microscope was used to characterize the roughness of four different surface structures. The experiment uses Sa, Sq and Sdq to characterize the roughness of different micro-nano structures.

Sdq is a parameter calculated by the root mean square of the slope of all points in the defined area. The more uneven the surface, the greater the value of Sdq.

$$S_{dq}=\sqrt{\frac{1}{A}\iint_A\left[\left(\frac{\partial z(x,y)}{\partial x}\right)^2+\left(\frac{\partial z(x,y)}{\partial y}\right)^2\right]dx\,dy} \tag{9}$$

It can be found from Fig. 13d that the roughness and surface fluctuation of the two-dimensional self-organized microholes structure are the largest, followed by the SWPSS and

mixed state structure of LIPSS+SWPSS. The roughness and surface undulation of LIPSS are smaller than the mixed state structure of LIPSS+SWPSS, SWPSS and self-organized microholes structure. The polished surface is the smoothest and the roughness is the smallest. In summary, it can be found that the two-dimensional structure has a greater value than the one-dimensional structure in terms of period, height profile, groove width and surface flatness. This discovery is very important for the study of the surface properties of amorphous alloys, especially the current research hotspot-the biocompatibility of amorphous alloys.

In addition, in order to verify whether the processing of zirconium-based amorphous materials by femtosecond laser radiation will result in the crystallization of bulk amorphous alloy materials. We performed X-ray diffraction tests on the original material and the material induced by the femtosecond laser. The structure is shown in Fig. 14, and it is found that when the femtosecond laser induces micro-nano texture on the zirconium-based amorphous surface, it does not crystallize it.

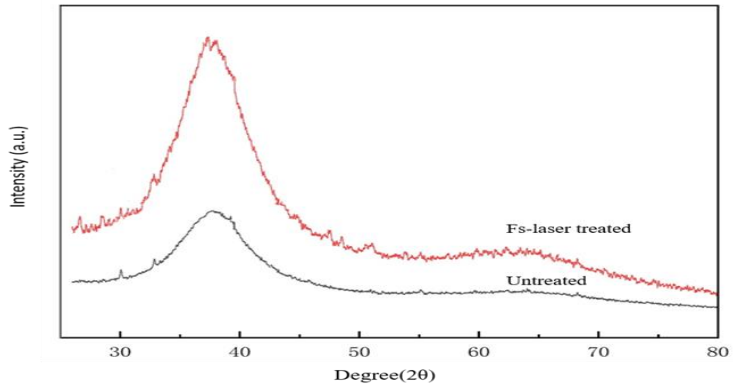

Figure 14 X-ray diffraction pattern of untreated and Fs-laser treated sample

3.4.2 Antibacterial properties

In order to verify the important effect of surface structure on the biological properties of the material. We cultured Escherichia coli on the surface of the sample to verify the influence of different structures on the adhesion of bacteria. The E.coli surface coverage morphology was observed under fluorescence microscopy after DAPI staining(Figure 15a). The surface bacterial coverage rate of specimens was calculated via gray analysis of fluorescence microscopy images(Figure15b). It can be seen that a large number of Escherichia coli are attached to the surface of the polished sample. The adhesion rate of E. coli on the surface of the polished sample

is 29.9%. The adhesion rate of bacteria on the surface of the LIPSS sample decreased significantly. Its adhesion rate of E. coli is 14.44%. The bacterial adhesion rate on the surface of the LIPSS+SWPSS sample continued to decrease. The bacterial adhesion rate of this structure sample is 8.33%. The bacterial adhesion rate on the surface of the SWPSS sample further decreased, and the bacterial adhesion rate decreased to 3.63%. The adhesion rate of Escherichia coli with self-organized microporous structure is the lowest, only 2.84%. It can be found that the surface roughness of the material and the antibacterial property show a certain positive ratio.

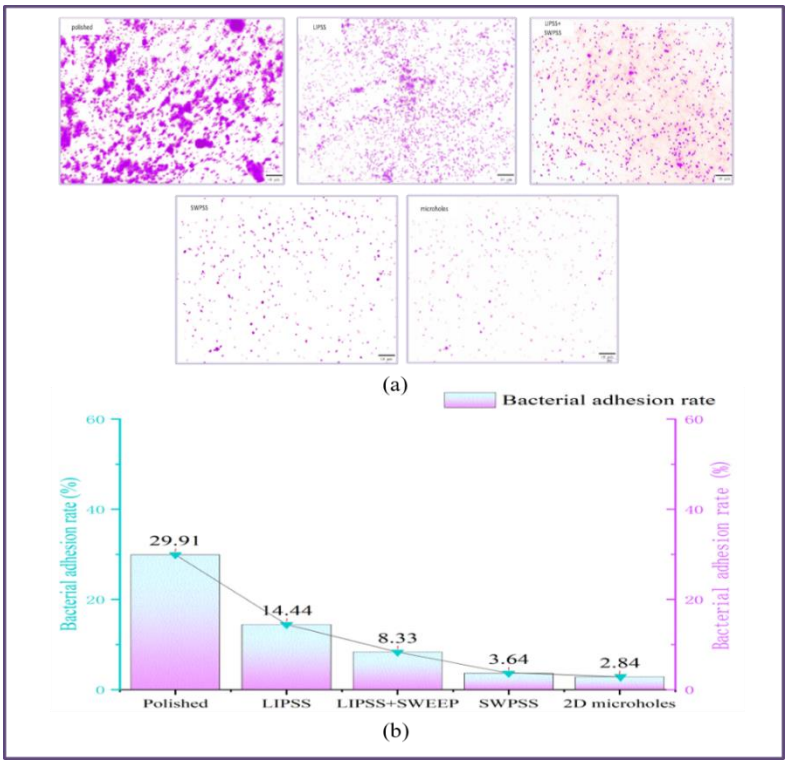

Figure 15 Surface adhesion of E.coli after 24h of incubation. (a)Fluorescence microscopy images of E.coli adhesion on specimen surfaces (b)surface bacterial coverage rate of specimens

4. Conclusion

(1) After optimizing the process parameters, one-dimensional LIPSS, LIPSS+SWPSS, SWPSS and two-dimensional self-organized microholes structure were induced on the surface of bulk amorphous alloy Zr55Cu16Ni15Ti10Al4, which avoided the crystallization of bulk amorphous alloy.

The self-organized microholes structure has the largest period and structure size, followed by SWPSS and LIPSS+SWPSS, and LIPSS is the smallest.

(2) It is found that within the appropriate process parameters, increasing the laser power,

pulse frequency, laser scan number and reducing the scanning speed will induce the micro-nano texture of the bulk amorphous alloy surface to transition from one-dimensional LIPSS to the mixed state of LIPSS+SWPSS, and converted into a SWPSS. Finally, the two-dimensional self-organized microholes structure is formed on the surface of the material. However, a small change of these process parameters will play a role in changing the amplitude on the original structure.

(3) The electromagnetic waves formed by the laser and the bulk amorphous alloy surface free electrons interfere with each other to cause the surface free electrons to produce periodic oscillations in density and temperature. Finally, electrons break down the material and "cold" etching produces striped LIPSS. As the effective accumulated fluence will continue to increase. The surface heat of the material is repeatedly superimposed to form a heat accumulation until the material's remelting threshold is exceeded. The ripple of the original LIPSS began to remelt slightly, and under the combined action of gravity and Marangoni thermal convection, a horizontal SWPSS was gradually formed. Finally, the effective accumulated fluence is further increased, the gravity and the surface tension at the micro-melt pool on the surface of the material reach a balance, and the two-dimensional self-organized pore structure is found on the base material.

(4) As LIPSS gradually transforms into a self-organized microholes structure, the roughness of the Zr-based metallic glasses surface gradually increases. Zr-based metallic glasses amorphous surface has gradually increased its ability to reduce the adhesion of E. coli. The self-organized microholes structure has the strongest ability to reduce E. coli adhesion. This research has important value for the application of Zr-based metallic glasses materials in the field of biomedicine.

Acknowledgments

This research was supported by National Natural Science Foundation of China (52075317, 51905333), the Royal Society through International Exchanges 2018 Cost Share (China) scheme (IEC\NSFC\181278).

References

[1] Li H F, Zheng Y F. Recent Advances in Bulk Metallic Glasses for Biomedical Applications[J]. Acta biomaterialia, 2016, 36:1-20.

[2] Nishiyama N, Amiya K, Inoue A. Recent progress of bulk metallic glasses for strain-sensing devices[J]. Materials Science & Engineering A, 2007, 449(none):79-83.

[3] Liu Z, Huang L, Wu W, et al. Novel low Cu content and Ni-free Zr-based bulk metallic glasses for biomedical applications[J]. Journal of Non-Crystalline Solids, 2013, 363:1-5.

[4] Buzzi S, Jin K, Uggowitzer P J, et al. Cytotoxicity of Zr-based bulk metallic glasses[J]. Intermetallics, 2006, 14(7):729-734.

[5] Li C, Zhang H, Cheng G, Faure N, et.al. Initial Cumulative Effects in Femtosecond Pulsed Laser-induced Periodic Surface Structures on Bulk Metallic Glasses [J]. Journal of Laser Micro Nanoengineering, 11.3(2015)357-365.

[6] Yang Jiao, Emmanuel Brousseau, Wayne Nishio Ayre. In vitro cytocompatibility of a Zr-based metallic glass modified by laser surface texturing for potential implant applications [J]. Applied Surface Science, 547(2021)149-194.

[4] H.F. Li, Y.F. Zheng. Recent advances in bulk metallic glasses for biomedical applications [J]. Acta Biomaterialia, 36(2016)1-20.

[5] E. Williamsa, N. Lavery. Laser processing of bulk metallic glass: A review [J]. Journal of Materials Processing Tech, 247(2017)73-91.

[6] Xiaoduo Wang, Haibo Yu, Peiwen Li, et.al. Femtosecond laser-based processing methods and their applications in optical device manufacturing: A review [J]. Optics and Laser Technology, 135(2021)106-687.

[7] Dezhi Tan, Kaniyarakkal N. Sharafudeen, et.al. Femtosecond laser induced phenomena in transparent solid materials: Fundamentals and applications [J]. Progress in Materials Science, 76(2016)154-228.

[8] Luo X, Yao S, Zhang H, et al. Biocompatible nano-ripples structured surfaces induced by femtosecond laser to rebel bacterial colonization and biofilm formation[J]. Optics & Laser Technology, 2020, 124:105973.

[8] Jian Cheng, Chang-sheng Liu, Shuo Shang, et.al. A review of ultrafast laser materials micromachining[J]. Optics & Laser Technology, 46(2013) 88-102.

[9] M. Birnbaum. Semiconductor surface damage produced by ruby lasers [J]. Appl

Phys, 36(1965)3688-3689.

[10] Tomokazu Sano, Kengo Takahashi, Akio Hirose, et.al. Femtosecond Laser Ablation of $Zr_{55}Al_{10}Ni_5Cu_{30}$ Bulk Metallic Glass [J]. Materials Science Forum Vols, 539-543(2007)1951-1954.

[11] Xinlin Wang, Peixiang Lu, Nengli Dai, et.al. Noncrystalline micromachining of amorphous alloys using femtosecond laser pulses [J]. Materials Letters, 61(2007)4290-4293.

[12] Fengxu Ma, Jianjun Yang, XiaonongZhu, et.al. Femtosecond laser-induced concentric ring microstructures on Zr-based metallic glass [J]. Applied Surface Science, 256(2010)3653-3660.

[13] L. Ran, S. Qu. Femtosecond laser induced surface structures on amorphous alloys [J]. 2011 Academic International Symposium on Optoelectronics and Microelectronics Technology, Harbin, 2011, pp. 134-137.

[14] Cezhi Du, Chengyong Wang, Tao Zhang, et.al. Reduced bacterial adhesion on zirconium-based bulk metallic glasses by femtosecond laser nanostructuring [J]. J Engineering in Medicine, 234.4(2019)095441191989801.

[15] Yuhao Lei, Jianjun Yanga,b, Cong Cong, et.al. Fabrication of homogenous subwavelength grating structures on metallic glass using double-pulsed femtosecond lasers [J]. Optics and Lasers in Engineering, 134(2020)106-273.

[16] Zhen Zhao, Bo Zhao, Yuhao Lei, et.al. Laser-induced regular nanostructure chains within microgrooves of Fe-based metallic glass [J]. Applied Surface Science, 529(2020)147-156.

[17] Tie Li, Yang Guo, Masayoshi Mizutani, et.al. Surface smoothing of bulk metallic glasses by femtosecond laser double-pulse irradiation [J]. Surface & Coatings Technology, 408(2021)126-803.

[18] Zhou Fang, Yuanan Zhao, Jianda Shao. Femtosecond laser-induced periodic surface structures on silica surface [J]. Optik, 127(2016)1171-1175.

[19] Z. M. Li, X. Wang, J. S. Nie. Formation of periodic ripples on silicon surface ablated by femtosecond laser [J]. Acta Physica Sinica, 66(2017)105-201.

[20] D Emmony, R Howson, L Willis. Laser mirror damage in germanium at 10.6 μm[J]. Applied Physics Letters, 23(1973)598-600.

[21] J. E. Sipe, Jeff F. Young, J. S. Preston, et.al. Laser-Induced Periodic Surface Structure. I.

Theory [J]. Physical Review B, 27(1983)1141-1154.

[22] J.Y. Thibault, J. Krüger, E. I. Tatiana, et.al. Rippled area formed by surface plasmon polaritons upon femtosecond laser double-pulse irradiation of silicon: the role of carrier generation and relaxation processes [J]. Applied Physics A, 117(2014)77–81.

[23] M. Barberoglou, G. D.Tsibidis, D. Gray, et.al. The influence of ultra-fast temporal energy regulation on the morphology of Si surfaces through femtosecond double pulse laser irradiation [J]. Applied Physics A, 113 (2013)273-283.

[24] G. D. Tsibidis, M. Barberoglou, P. A. Loukakos. Dynamics of ripple formation on silicon surfaces by ultrashort laser pulses in subablation conditions [J]. Physical Review, 86(2012)115316.1-115316.14.

[25] George D. Tsibidis, Evangelos Skoulas, Antonis Papadopoulos, et.al. Convection roll-driven generation of supra-wavelength periodic surface structures on dielectrics upon irradiation with femtosecond pulsed lasers [J]. Phys. Rev. B 94, 081 (2016)-305.

[26] G. D. Tsibidis, C. Fotakis, E. Stratakis. From ripples to spikes: A hydrodynamical mechanism to interpret femtosecond laser-induced self-assembled structures [J]. Physical Review B 92, 041405 (2015).

[27] M. Huang, F. Zhao, Y. Cheng, et al. Origin of Laser-Induced Near-Subwavelength Ripples: Interference between Surface Plasmons and Incident Laser [J]. Acs Nano, 3(2009)4062-4070.

[28] B.N. Chicbkov, C. Momma, S. Nolte, et.al. Femtosecond, picosecond and nanosecond laser ablation of solids [J]. Applied Physics A, 63(1966)109-115.

[29] Zijlstra P. Photothermal properties of gold nanorods and their application to five-dimensional optical recording [D]. Melbourne: Swinburne University of Technology, 2009.

[30] Junke Jiao, Xinbing Wang. A numerical simulation of machining glass by dual CO_2-laser beams [J]. Optics & Laser Technology, 40 (2008) 297–301.

[31] Liyang Yue, Zengbo Wang, Lin Li. Modeling and simulation of laser cleaning of tapered micro-slots with different temporal pulses [J]. Optics & Laser Technology, 45 (2013) 533–539.

[32] Fotios Frangelakis. Controlling and upscaling laser induced surface morphology: from tens of microns to tens of nanometres. Micro and nanotechnologies/Microelectronics [D]. Université de Bordeaux, 2019. English. ffNNT: 2019BORD0021ff. fftel-02259929f.